CONF-960448--13

HYDRAULICALLY POWERED DISSIMILAR TELEOPERATED SYSTEM CONTROLLER DESIGN*

John F. Jansen
Robotics and Process Systems Division
Oak Ridge National Laboratory†
Post Office Box 2008
Oak Ridge, Tennessee 37831-6304

Reid L. Kress
Robotics and Process Systems Division
Oak Ridge National Laboratory†
Post Office Box 2008
Oak Ridge, Tennessee 37831-6304

To be presented at the
1996 IEEE International Conference on
Robotics and Automation
Minneapolis, Minnesota
April 22-28, 1996

*Research sponsored by the Robotics Technology Development Program, U.S. Department of Energy, under contract DE-AC05-84OR21400 with Lockheed Martin Energy Research Corp.

† Oak Ridge National Laboratory, managed by Lockheed Martin Energy Research Corp. for the U.S. Department of Energy under contract number DE-AC05-96OR22464.

Hydraulically Powered Dissimilar Teleoperated System Controller Design

John F. Jansen and Reid L. Kress
Robotics & Process Systems Division
Oak Ridge National Laboratory
Oak Ridge, TN 37831-6304

Abstract

This paper will address two issues associated with the implementation of a hydraulically powered dissimilar master-slave teleoperated system. These issues are the overall system control architecture and the design of robust hydraulic servo controllers for the position control problem. Finally, a discussion of overall system performance on an actual teleoperated system will be presented. (Schilling's Titan II hydraulic manipulators are the slave manipulators and the master manipulators are from the Oak Ridge National Laboratory-developed Advanced Servo Manipulator.)

1. Introduction

Many tasks slated for manipulators are highly unstructured (e.g., complicated assembly tasks, disassembly of unknown or sophisticated hardware, survey and characterization operations, clean-up of hazardous materials, etc.) and do not lend themselves to autonomous implementation. Often, operating procedures and regulatory requirements dictate that the decision-making process be retained with a human operator. As a result of the need to maintain operator control, teleoperator development began in the 1950's with Ray Goertz [Goertz,54], continued through the 1960's with Carl Flatau [Flatau,65], and is sustained today with a myriad of other contributors. This paper discusses the controller design for a new teleoperated system developed at Oak Ridge National Laboratory (ORNL). The paper is organized as follows: after the introduction is a section on the overview of the teleoperated system and its controller architecture. Next are sections on the servo and joint controllers, followed by results and conclusions.

2. Overview of Hardware and Software

2.1 Overview of Selective Equipment Removal System

The Selective Equipment Removal System (SERS) is a reconfigurable and modular deployment system for the dual-arm work module (DAWM), which is a generic manipulation package designed to provide both dexterous teleoperation and robotic capability (only teleoperation will be addressed in this paper). The SERS is specifically designed to study and address the needs of facility decontamination and dismantlement (D&D). Multiple deployment options are provided to support the needs of different facilities. Some sites may have overhead cranes available. The initial implementation of SERS uses a rigid boom gantry overhead transporter system located in the Robotics and Technology Assessment Facility at ORNL. The transporter provides X, Y, Z, and boom rotation functions for gross positioning of the DAWM (Fig. 1). The DAWM consists of a 5-degree-of-freedom (5-dof) base manufactured by RedZone Robotics and two 6-dof Schilling manipulator arms. The Schilling arms serve as the slaves of the teleoperated system. The Schilling manipulators (Fig. 2) are servovalve-controlled, hydraulically-actuated manipulators with a supply side pressure of 3000 psi. These manipulators provide higher lift capacity than that normally available for dexterous teleoperation with 240 lb in the elbows-up configuration dropping to 150 lb in the elbows-out configuration. Joint positions are measured by 12-bit resolvers and a linear variable differential transformer is used to indicate gripper position. A six-axis force/torque sensor is located in the wrist of each arm. Presently the existing force/torque sensors have significant noise and offset.

For teleoperation, the master arms which serve as the operator interface to the DAWM are the master manipulator hardware converted from the Advanced Servo Manipulator (ASM), a manipulator designed at ORNL [Kuban,84] and extensively tested in the 1980's [Draper,89] (Fig. 3). The ASM is a fixed configuration, elbows-down, remotely maintainable manipulator that was designed to meet the needs of fuel reprocessing facilities. The master manipulator achieves torque transmission via tensioned steel cables.

The computer controller is VME-bus based and uses five Motorola 68030-based single board computers in the same back plane. One CPU handles each of the master controller arms and slave manipulators and runs synchronous deterministic control loops. The fifth CPU is used for asynchronous communications to the operator interface and various facility support equipment where loop rate requirements are not stringent. Control is actually handled through two VME back planes separated by 300 ft and connected by a bus repeater card set through a set of four optical fibers. Control and sensor communication for all manipulator parameters is managed through a custom Schilling VME bus card and electronics module for each manipulator. All CPU's are

located in the master rack in the control room. Only the bus repeater cards and I/O cards relevant to DAWM control are located in the back plane in the DAWM. All software is done in C or C++ and modules run under Wind River's VxWorks® real-time control architecture.

The manipulators are run continuously in the impedance control mode in teleoperation and adjusted to be stiff or compliant as the task requires. High compliance in one manipulator is a useful mode when executing coordinated two-arm tasks robotically. Certain types of tasks, such as peg-in-hole, are best completed in an impedance control mode where the remote compliance center [Whitney,82] can be altered in addition to the compliance matrix.

The initial operator interface makes use of the existing ASM Advanced Integrated Maintenance System (AIMS) video console which includes three 19-in. video views and six 9-in. video views. Future development will examine alternate viewing schemes focusing on those methods which will accommodate extended use by operators. Operator interface menus are provided by Sun workstation X-Window-based graphics and a Silicon Graphics machine running IGRIP for 3-D modeling of the task space and displaying DAWM orientations.

DAWM will have a collection of tools to address D&D tasks. Power tools include impact wrenches, grinders, cut-off saws, and a stainless steel wet/dry vacuum cleaner. A previously modified Hurst "Jaws-of-Life"® hydraulic cutter, originally designed for rescuing injured passengers from automotive accidents, was refitted to the overhead transporter and made available to the DAWM (Fig. 4). Long-term goals have been identified to pursue plasma-arc cutting, high-pressure water cutting, CO_2 blasting, as well as other technologies necessary for large scale dismantlement of structures not designed for remote interaction.

2.2 Overview Control Architecture

Position-Force control is the strategy selected for the Titan II manipulators and the ASM masters for several reasons. First, the Titan II joints are not backdrivable (i.e., large joint friction exists in each joint). Second, the Force/Torque sensors (JR3) for each arm are on the wrist (i.e., no joint torque measurements). Third, the kinematics between the ASM master arms and the Schilling slave arms are dissimilar. This last reason was probably the most critical because the two manipulators (master and slave) in this paper are not anthropomorphic, a Cartesian (i.e., x, y, z and Euler parameters) based scheme was chosen instead of a standard joint-to-joint type of controller. The master manipulators have a shoulder pitch, shoulder roll, elbow pitch, and a 3-dof spherical wrist (i.e., pitch, yaw, and roll). The slave manipulators have a shoulder azimuth (yaw), shoulder elevation (pitch), elbow pitch, and a wrist pitch and yaw (whose axes do not intersect) and a wrist roll. Furthermore, the relative link lengths of the master and slave manipulators are significantly different (e.g., the first two link lengths of the ASM master manipulators are 25 and 20 in. plus an offset of 1.125 in. and the first two link lengths of the Schilling Titan II slave manipulators are 33.5 and 19 in.). Also, Cartesian control has the advantage that the master manipulator controller software can be the same for teleoperation and for robotic operation. Only the software front end changes as to whether the master controller or a trajectory planner is driving the slave manipulator end effector.

Typically, joint position-position control strategies have been utilized in the past [Goertz,54]; however, the control architecture (Fig. 5) for DAWM is a position-force type controller where Cartesian position from the master arm is transmitted to the slave manipulator and the slave's force signal is transmitted back to the master arm. The position-force control architecture was first demonstrated by Flatau [Flatau,65]. Briefly, the following is a summary of the function performed by each routine in the block diagram of Fig. 5.

1. inv_kin_t2() - inverse kinematic routine for the Schilling Titan II slave manipulator
2. kin_joint_t2() - kinematic routine for the Schilling Titan II slave manipulator
3. jr3_to_tool() - converts the force/torque signal to tool frame at the gripper. (The force/torque sensor *is manufactured by JR3, Inc.)*
4. impedance_control() - simple impedance controller
5. indexing and move wrist are both associated with indexing of the master/slave manipulators
6. motor_torque_to_current() - converts the torque commands to current commands
7. kin_joint_Jac_Force_asm() - combines the software for the kinematic routine and the manipulator Jacobian code for the master manipulator into one routine
8. motor_to_JtAngle() - converts motor angles to joint angles (this is needed since this is a cable-driven system)
9. Sensor _to_Gripper_Force() and force_reflection ratio - converts the force/torque sensor signal to gripper forces and moments and then multiples results with the desired force_reflection ratio required by the operator.
10. force_filter() - due to the noise level on the force/torque sensor, a second order lag filter is utilized with a bandwidth set at 4Hz.
11. grav_comp() - removes the gravitational component from the force/torque signal. The input signal (angle_RedZone) is the angle from the 5-dof DAWM base manufactured by RedZone Robotics, Inc.

12. jr3_calibration() - using a least-mean squares algorithm, the bias and scale factor for the force/torque sensor (with the exception of the wrist roll) is estimated at the startup of the slave manipulators. The bias settings will change due to the residual hydraulic fluid pressure in the hydraulic lines that pass through the force/torque sensor.
13. servo_comp() - low level joint hydraulic servo controller.

Only the servo_comp routine will be addressed in the rest of this paper since it is fundamental to all of the other control loops in the system. It is shown as the shaded block in Fig. 5.

3. Servo Controller Design and Joint Modeling

Servo control of hydraulic-based systems can achieve similar positional tracking accuracies as more common electric-based drive systems; however, there are noticeable problems that have to be overcome. The low-level joint controller design construction is based on overcoming the following types of nonlinearities: Coulomb and stick-slip type of friction, orifice governing equation of the servovalves, changes in fluid properties with time and temperature (i.e., effective bulk modulus), and changing inertia parameters of the manipulator in different postures. The controller had to be robust to these large nonlinear forces.

Groups of linear models have been used to characterize the manipulator performance and to aid in the controller design. Linear models were used based on transfer functions derived in [Merritt,67] and derived from measured data [Braun,87]. The most significant nonlinear effects were joint friction (around 10 to 20 percent of the joint torque capacity) and drive train compliance. Describing function techniques [Gelb,68] were adequate to completely predict when a limit cycle would occur. Since describing function techniques are a frequency-based method, Nichols plots were heavily used in the design process. Figure 6 shows the block diagram of the joint controller. In Fig. 6, A is the actuator area, β_e is the effective bulk modulus, G_c is the joint compensator (designed in the following section), A is the actuator area, V_T is the total system volume, M is the system mass, C_{tp} is the total leakage flow, Kp is the pressure gain of the servovalve, K_q is the flow gain of the servovalve, R is the effective resistance of the servovalve, and F_{frict}, F_{Load}, F_{grav}, are the friction, load, and gravity forces respectively. Table 1 shows the experimentally determined transfer function for the elbow joint of the left Titan II slave manipulator. The elbow joint is analyzed exclusively in the following discussion because it was representative of the procedure used for all of the Schilling Titan II joints and exhibited the most severe control challenges. The transfer function relates the joint position in radians to the command signal in counts with a 12-bit D/A board. The hydraulic servo valve and joint transfer function plant models are for different arm postures and for different command levels. A sinusoidal command was given and slowly swept through the frequency range of interest. Note that the pole locations and the dc velocity gain varies significantly (the dc velocity gain varies as much as 50 percent) throughout the workspace, for different command levels, and under different operating conditions (initial operation at cold start-up with entrapped air changing to a condition with the fluid at thermal equilibrium and the entrapped air washed out of the system). The operating conditions have a significant affect on the effective bulk modulus (β_e) of the fluid. In Fig. 7, the data clearly indicates the excellent match between the model (shown as the lines) and the experimental data (points marked with an x). (The joint used to obtain the data in Fig. 7 is the same as the joint used to determine the transfer functions of Table 1.) The amplitude plot contains the amplitude of the data points and transfer functions. Data and experimentally determined transfer function amplitudes match very well. In the phase plot, the transfer function plots and the data exhibit the low-frequency performance expected of a type 1 system (-90 degree phase shift); however, at the higher frequencies, data are up to 20 degrees off of the model in the lagging direction. The primary reasons for the additional lag in the data are unmodelled dynamics, such as nonlinear friction with hysteresis in the hydraulic system. (Matching amplitude and lagging phase is typical for a nonlinearity containing area like hysteresis or nonlinear friction. Matching phase and not matching amplitude is typical for a nonlinearity containing no area such as saturation or deadband.) Figure 7 validates the use of the models for controller design.

4. Joint Compensators

The goal in the design of the joint compensators was to use frequency response information to shape the response of the joint plant and joint compensator so that the controller would remain robust to large plant variations but avoid high-amplitude limit cycles resulting from significant nonlinearities, such as joint friction (typical of hydraulically actuated manipulators). Large plant variations result from changes in the hydraulic properties because of temperature variation during warm-up and operation, as well as changing manipulator configuration, picking up payloads, and contact with different environments.

For all of the Schilling Titan II slave manipulator joints the joint natural frequencies were under 8 Hz and, therefore, a sampling rate of 120 Hz was used for the slave manipulators (sampling at a factor of 15 times the

natural frequency). For the master manipulators, the highest bandwidth is under 4 Hz indicating that a sampling rate of 60 Hz would be adequate; however, a sampling rate of 200 Hz was selected where the increased rate was necessary due to the rollover effect of the resolvers used as joint position sensors. As a result of the low plant bandwidths, the analysis for the controller was performed in the s-domain and not the z-domain (we could have converted to the w-domain [Chen,89] as other researchers have done, but this rigor was not necessary). Transfer functions and analysis in the s-domain have been used by other researchers to design controllers for hydraulically actuated manipulators [Habibi,95]. The compensator design steps are numbered in the following discussion.

1) To achieve the dc stiffness requirements (i.e., joint deflection for rated load), a dc-gain of 10,000 was required for the joint compensator. Nonlinear effects such as joint friction were the dominant drivers in the compensator design and these are easiest to analyze in the frequency domain. Figure 8 shows the Nichols plot of the model of the elbow joint of the Schilling Titan II slave manipulator, having joint compliance, with varying ratios of stiction to Coulomb friction. Figure 8 was made using the describing function method outlined in Merritt [Merritt, 67, pp. 304-16]. The lines of Fig. 8 are for friction ratios (Stiction/Coulomb) of 1.0, 1.1, 1.25, 1.5, 2, 3, 5, and 10 respectively, going from the top to the bottom. Because the joint is a type 1 system, its frequency response will approach the -90 degree open-loop phase line at low frequencies. Clearly the system response will intersect the nonlinear friction describing function curves indicating a limit cycle exists. Because the system response approaches -270 degree phase lag at high frequencies, increasing the size of the stiction relative to the Coulomb friction increases the amplitude of the limit cycle; however, compensating the response of the joint to move the intersection of the compensator plus plant response with the describing function curve farther to the right (closer to the -90 degree phase line) lowers the amplitude of the limit cycle. This is one objective of the compensator.

2) To provide adequate robustness margins to the possible variations in nonlinear friction as well as to plant operating conditions such as payload, configuration, and environmental impedance, the following compensator was selected:

$$G_c(s) = 10{,}000\,\frac{\left(\frac{s}{0.2}+1\right)}{\left(\frac{s}{0.06}+1\right)}\,\frac{1}{\frac{s}{15}} + \frac{K_I}{s} \qquad (1)$$

The compensator provides lag at 0.06 and 15 rad/s and lead at 0.2 rad/s.

3) To increase the order of the compensator to make the steady-state error return to zero, a small integration gain, K_I, has been added. The value of K_I was set very low (~100) because it tended to increase the limit cycle amplitude. An antiwindup feature was added, which limited the maximum value of the integral term and provided for the immediate reduction of the integral when the error signal changed sign.

Figure 9 shows the Nichols plot of the model of the Schilling Titan II elbow joint with the compensator of Eq. (1). The compensator provided low-frequency lag (0.06 rad/s break frequency) and lead at moderate frequencies (0.2 rad/s break frequency), thereby shaping the compensated response of the system around the -1 point (0 db, -180 degrees on the Nichols plot). The compensated response "hugs" the -90 degree open-loop phase line for moderate frequencies, thereby reducing the amplitude of the nonlinear friction-induced limit cycles. "Hugging" the -90 degree open-loop phase line also provides almost 90 degrees of phase margin (observe the distance between the system response curve and the -1 point measured along the 0 db open-loop gain line). This phase margin for the compensated model response is desirable when one considers the results of Fig. 7 where actual system response lags the modeled response by an additional 20 degrees (forcing the response closer to the -1 point on the Nichols plot). At higher frequencies, the compensator provides additional lag (15 rad/s break frequency). This serves to move the point where the system models spread out farther to the left in the Nichols plot. The "spreading out" is a result of changes in the plant parameters and the compensator goal is to have at least a 20-db gain margin (observe the distance between the compensated response curve and the -1 point measured along the -180 degree open-loop phase line) so that the compensated system is robust to plant variations even of an order of magnitude.

4) As expected, small limit cycles at low frequency have been observed on some of the joints (elbow, wrist pitch, and wrist yaw), which is typical of other hydraulically actuated systems [Mougenet,95]. These limit cycles can be reduced by careful design to a level where they are not visible.

5) The drive signal must be constrained to avoid actuator saturation. Following similar lines as those taken in Quantitative Feedback Theory [Horowitz,72], the drive constraint must satisfy the following inequality:

$$\left|\frac{G_c}{1 + G_c P}\right| \theta_{max}^{cmd} \le 1000 \text{ cts} \qquad (2)$$

natural frequency). For the master manipulators, the highest bandwidth is under 4 Hz indicating that a sampling rate of 60 Hz would be adequate; however, a sampling rate of 200 Hz was selected where the increased rate was necessary due to the rollover effect of the resolvers used as joint position sensors. As a result of the low plant bandwidths, the analysis for the controller was performed in the s-domain and not the z-domain (we could have converted to the w-domain [Chen,89] as other researchers have done, but this rigor was not necessary). Transfer functions and analysis in the s-domain have been used by other researchers to design controllers for hydraulically actuated manipulators [Habibi,95]. The compensator design steps are numbered in the following discussion.

1) To achieve the dc stiffness requirements (i.e., joint deflection for rated load), a dc-gain of 10,000 was required for the joint compensator. Nonlinear effects such as joint friction were the dominant drivers in the compensator design and these are easiest to analyze in the frequency domain. Figure 8 shows the Nichols plot of the model of the elbow joint of the Schilling Titan II slave manipulator, having joint compliance, with varying ratios of stiction to Coulomb friction. Figure 8 was made using the describing function method outlined in Merritt [Merritt, 67, pp. 304-16]. The lines of Fig. 8 are for friction ratios (Stiction/Coulomb) of 1.0, 1.1, 1.25, 1.5, 2, 3, 5, and 10 respectively, going from the top to the bottom. Because the joint is a type 1 system, its frequency response will approach the -90 degree open-loop phase line at low frequencies. Clearly the system response will intersect the nonlinear friction describing function curves indicating a limit cycle exists. Because the system response approaches -270 degree phase lag at high frequencies, increasing the size of the stiction relative to the Coulomb friction increases the amplitude of the limit cycle; however, compensating the response of the joint to move the intersection of the compensator plus plant response with the describing function curve farther to the right (closer to the -90 degree phase line) lowers the amplitude of the limit cycle. This is one objective of the compensator.

2) To provide adequate robustness margins to the possible variations in nonlinear friction as well as to plant operating conditions such as payload, configuration, and environmental impedance, the following compensator was selected:

$$G_C(s) = 10{,}000\,\frac{\left(\frac{s}{0.2}+1\right)}{\left(\frac{s}{0.06}+1\right)}\,\frac{1}{\frac{s}{15}} + \frac{K_I}{s} \qquad (1)$$

The compensator provides lag at 0.06 and 15 rad/s and lead at 0.2 rad/s.

3) To increase the order of the compensator to make the steady-state error return to zero, a small integration gain, K_I, has been added. The value of K_I was set very low (~100) because it tended to increase the limit cycle amplitude. An antiwindup feature was added, which limited the maximum value of the integral term and provided for the immediate reduction of the integral when the error signal changed sign.

Figure 9 shows the Nichols plot of the model of the Schilling Titan II elbow joint with the compensator of Eq. (1). The compensator provided low-frequency lag (0.06 rad/s break frequency) and lead at moderate frequencies (0.2 rad/s break frequency), thereby shaping the compensated response of the system around the -1 point (0 db, -180 degrees on the Nichols plot). The compensated response "hugs" the -90 degree open-loop phase line for moderate frequencies, thereby reducing the amplitude of the nonlinear friction-induced limit cycles. "Hugging" the -90 degree open-loop phase line also provides almost 90 degrees of phase margin (observe the distance between the system response curve and the -1 point measured along the 0 db open-loop gain line). This phase margin for the compensated model response is desirable when one considers the results of Fig. 7 where actual system response lags the modeled response by an additional 20 degrees (forcing the response closer to the -1 point on the Nichols plot). At higher frequencies, the compensator provides additional lag (15 rad/s break frequency). This serves to move the point where the system models spread out farther to the left in the Nichols plot. The "spreading out" is a result of changes in the plant parameters and the compensator goal is to have at least a 20-db gain margin (observe the distance between the compensated response curve and the -1 point measured along the -180 degree open-loop phase line) so that the compensated system is robust to plant variations even of an order of magnitude.

4) As expected, small limit cycles at low frequency have been observed on some of the joints (elbow, wrist pitch, and wrist yaw), which is typical of other hydraulically actuated systems [Mougenet,95]. These limit cycles can be reduced by careful design to a level where they are not visible.

5) The drive signal must be constrained to avoid actuator saturation. Following similar lines as those taken in Quantitative Feedback Theory [Horowitz,72], the drive constraint must satisfy the following inequality:

$$\left|\frac{G_C}{1 + G_C P}\right| \left|\theta^{cmd}_{max}\right| \le 1000 \text{ cts} \qquad (2)$$

where 1000 cts is roughly half (picked for conservatism) of the 12-bit range of the D/A card (2^{12} implies ±2048) and $|\theta^{cmd}_{max}|$ was selected to be 5 degrees. The above constraint was plotted and is shown in Fig. 10. The peak for each model was below 60 dB (i.e., under 1000) and therefore saturation is avoided.

5. Summary/Conclusion

This paper discussed the modeling and experimental development of a servo controller for a hydraulically actuated teleoperator system. Servo control of hydraulic-based systems can achieve similiar positional tracking accuracies as more common electrically actuated drive systems; however, there are noticeable problems that have to be overcome to achieve similiar tracking performances. In designing the low-level joint controller, Coulomb friction and stick-slip type of friction nonlinearities, as well as the nonlinearities resulting from the hydraulic system (orifice governing equation of the servovalves, changes in fluid properties with time and temperature; i.e., effective bulk modulus) and nonlinearly varying inertia parameters of the manipulator had to be overcome. Groups of linear models were used to characterize the manipulator performance and to aid in the controller design. Applying the controllers to the teleoperated slave manipulators resulted in a very stiff system under all payload and operating conditions. The manipulators remain stable and the controllers are robust to system variations during extended operations. The arms and controllers have been used successfully through many hours of D&D operation.

Acknowledgements

The authors would like to acknowledge the support of the Department of Energy Robotics Technology Development Program headed by Dr. Lin Yarbrough.

References

[Braun,87] Braun, S. G. and Ram, Y. M., "Structural Parameter Identification in the Frequency Domain: The Use of Overdetermined Systems," J. of Dyn. Sys. Meas. and Control, Vol. 109, June 1987, pp. 120-23.

[Chen,89] Chen, Y., "Replacing a PID Controller by a Lag-Lead Compensator for a Robot-A Frequency Response Approach," IEEE Trans. on Rob. and Auto., Vol. 5, No. 2, April 1989, pp. 174-82.

[Draper,89] Draper, J. V., Schrock, S. L., and Handel, S. J., "Performance Evaluation of the Oak Ridge National Laboratory's Advanced Servomanipulator," Proc. of ANS Third Topical Meeting on Robotics and Automation, March 13-16, 1989, Charleston, SC.

[Flatau,65] Flatau, C. R., "Development of Servo Manipulators for High Energy Accelerator Requirements," Proc. 13th, Conf. on Remote Systems Technology, 1965, pp. 29-35.

[Gelb,68] Gelb, A. and Velde, W. E. V., Multiple-Input Describing Functions and Nonlinear System Design, McGraw-Hill, Inc., New York, NY, 1968.

[Goertz,54] Goertz, R. C. and Thompson, W. M., "Electronically Controlled Manipulator," *Nucleonics*, Nov. 1954, pp.46-47.

[Habibi,95] Habibi, S. R. and Goldenberg, A. A., "Design and Control of a Reconfigurable Industrial Hydraulic Robot," Proc. of IEEE Int. Conf. on Rob. and Auto., May 21-27, 1995, Nagoya, Japan, pp. 2206-11.

[Horowitz,72] Horowitz, I. M. and Sidi, M., "Synthesis of Feedback Systems with Large Plant Ignorance for Prescribed Time-Domain Tolerances," Int. J. Control, Vol. 16, Feb. 1972, pp. 287-309.

[Kuban,84] Kuban, D. P. and Perkins, G. S., "Dual Arm Master Controller Concept," Proc. of the ANS Topical Meeting on Robotics and Remote Handling in Hostile Environments, American Nuclear Society, 1984, pp. 433-37.

[Merritt,67] Merritt, H. E., Hydraulic Control Systems, John Wiley & Sons, New York, NY, 1967.

[Mougenet,95] Mougenet, F. and Hayward, V., "Limit Cycle Characterization, Existence and Quenching In the Control of a High Performance Hydraulic Actuator," Proc. of IEEE Int. Conf. on Rob. and Auto., May 21-27, 1995, Nagoya, Japan, pp. 2218-23.

[Whitney,82] Whitney, D. E., "Quasi-Static Assembly of Compliantly Supported Rigid Parts," J. Dyn Sys. Meas. and Control, Vol. 104, March 1982, pp. 64-77.

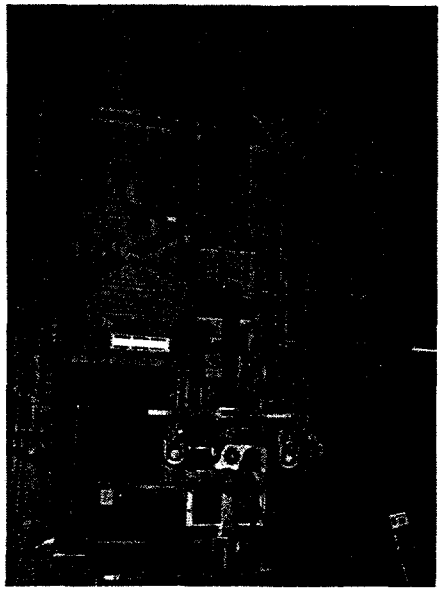

Fig. 1. SERS transporter for the DAWM.

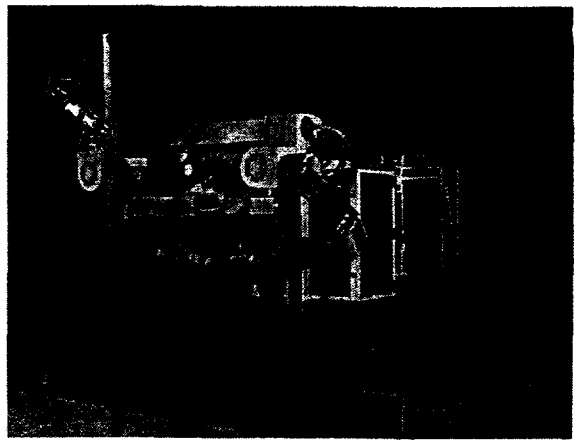

Fig. 2. The DAWM showing the Schilling manipulator arms.

Fig. 3. The Advanced Servo Manipulator master arms.

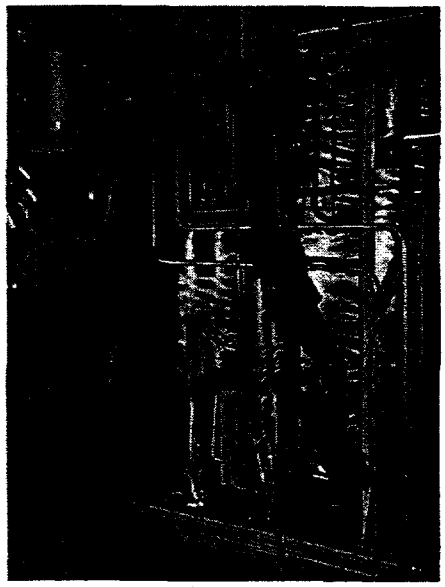

Fig. 4. DAWM with "Jaws-of-Life" hydraulic cutter.

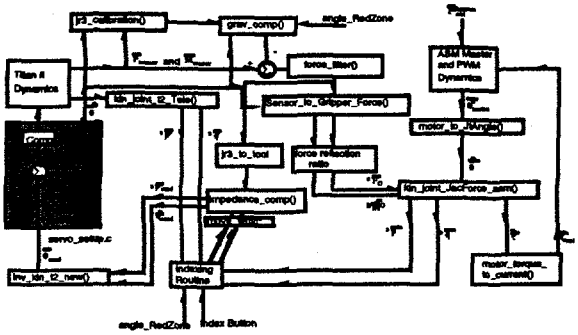

Fig. 5. Teleoperation block diagram for position-force control.

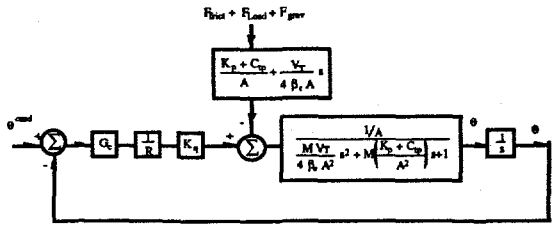

Fig. 6. Block diagram of the joint controller.

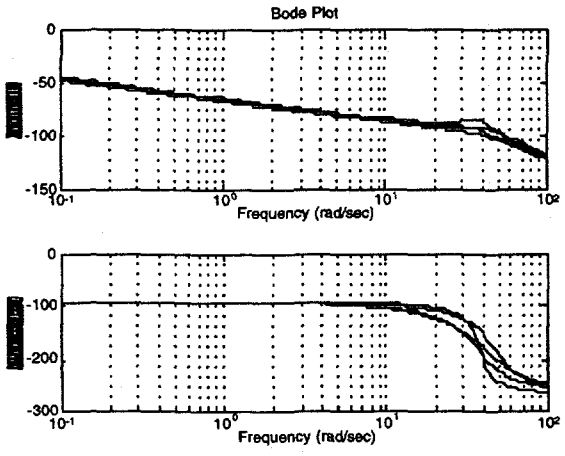

Fig. 7. Model and experimentally determined amplitude and phase for the elbow joint of the Schilling Titan II slave manipulator.

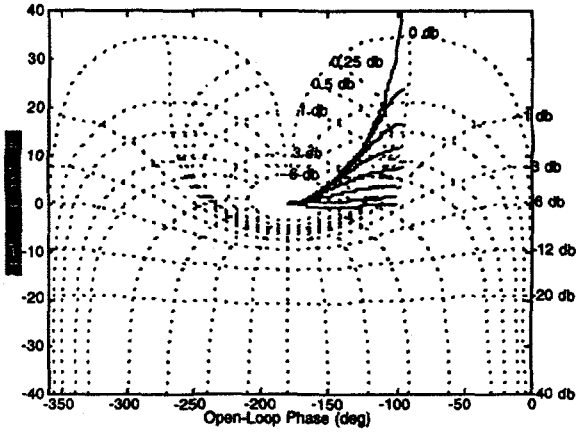

Fig. 8. Nichols plot of the model for the elbow joint of the Schilling Titan II slave manipulator showing the effect of joint nonlinear friction and compliance on stability (Describing function method).

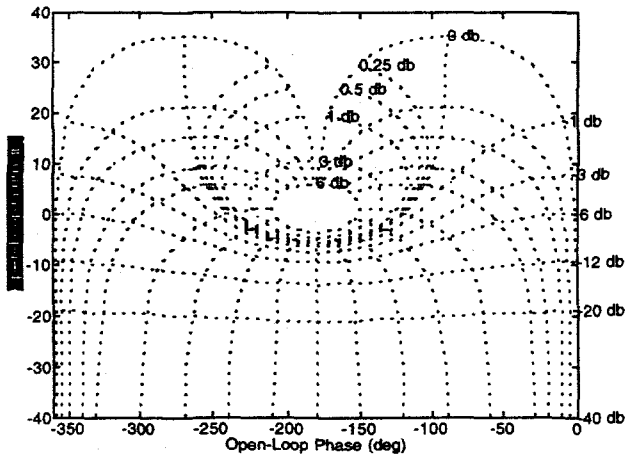

Fig. 9. Nichols plot of the plant model of Fig. 6 with the compensator, G_C, of Eq. 1.

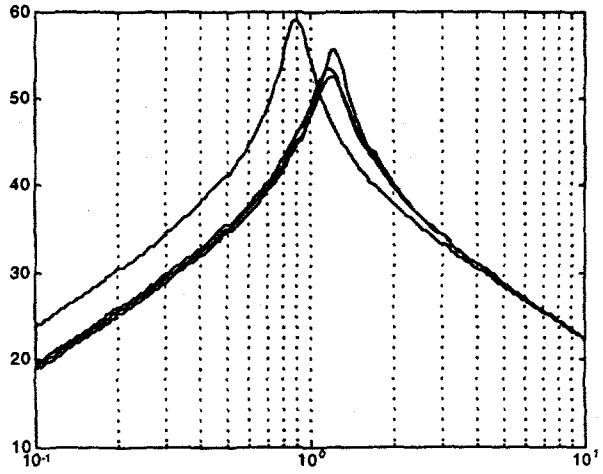

Fig. 10. Magnitude of (dB) versus frequency (rad/s) showing how the 1000 count (60 dB) constraint is avoided for all frequencies (Drive signal boundary).

Table 1. Experimentally determined transfer function for the elbow joint of the left Schilling Titan II slave manipulator.

Plant #	Transfer Function	Pole Location
1	$\frac{0.0005311}{0.0007501\ s^3 + 0.01935\ s^2 + s}$	0; -12.897± 34.160i
2	$\frac{0.0006001}{0.0007029\ s^3 + 0.007587\ s^2 + s}$	0; -5.397± 37.330i
3	$\frac{0.0004086}{0.0006057\ s^3 + 0.02369\ s^2 + s}$	0; -19.557± 35.614i
4	$\frac{0.0005094}{0.0004542\ s^3 + 0.01264\ s^2 + s}$	0; -13.911± 44.815i